SAND2010-7526C
LLNL-0868

Effects of Post-Injection Strategies on Near-Injector Over-Lean Mixtures and Unburned Hydrocarbon Emission in a Heavy-Duty Optical Diesel Engine

Author, co-author list (Do NOT enter this information. It will be pulled from participant tab in MyTechZone)

Affiliation (Do NOT enter this information. It will be pulled from participant tab in MyTechZone)

ABSTRACT

Post-injection strategies aimed at reducing engine-out emissions of unburned hydrocarbons (UHC) were investigated in an optical heavy-duty diesel engine operating at a low-load, low-temperature combustion (LTC) condition with high dilution (12.7% intake oxygen) where UHC emissions are problematic. Exhaust gas measurements showed that a carefully selected post injection reduced engine-out UHC emissions by 20% compared to operation with a single injection at the same load. High-speed in-cylinder chemiluminescence imaging revealed that without a post injection, most of the chemiluminescence emission occurs close to the bowl wall, with no significant chemiluminescence signal within 27 mm of the injector. Previous studies have shown that over-leaning in this near-injector region after the end of injection causes the local equivalence ratio to fall below the ignitability limit. With a carefully selected post-injection, mixtures close to the injector show significant chemiluminescence emission, indicating more complete combustion of those regions, likely due to increased local equivalence ratios.

Simultaneous planar laser-induced fluorescence (PLIF) of OH with 284-nm excitation and PLIF of combined formaldehyde and polyaromatic hydrocarbons (PAH) with 355-nm excitation were employed to identify the regions of first- and second-stage ignition, as well as providing some indication of local equivalence ratios. The laser diagnostics show that without a post injection, regions close to the injector show formaldehyde fluorescence late in the cycle without detectable OH fluorescence, indicating that these regions do not achieve second-stage ignition, and therefore likely contribute to UHC emissions. Persistence of formaldehyde fluorescence late in the cycle is also consistent with fuel-lean mixtures. With a carefully selected post injection, strong OH fluorescence appears in the near-injector regions, indicating that they are likely enriched by the post-injection such that they reach second-stage ignition and more complete oxidation. The reduction observed in the exhaust UHC emission is therefore attributed to the enrichment mechanism of the near-injector regions by the close-coupled post-injection.

INTRODUCTION

The past decade has seen tremendous development in diesel engine technology and performance in response to ever more stringent emissions legislations. Heavy-duty diesel engines have significantly reduced their emissions of nitrous oxides (NO_X) and particulate matter (PM). Low temperature combustion (LTC) is one way of improving the NO_X/PM tradeoff by dilution of the charge with large amounts of cooled exhaust gas recirculation (EGR). The dilution with EGR keeps the adiabatic flame temperature below the thermal NO_X formation temperature region and decreases soot formation [1]. In the lower load range, ignition typically occurs after the end of injection (EOI), so that the ignition dwell, which is the time from EOI to the start of combustion, is positive. The ignition dwell is usually longer at lower loads, in part because the injection duration is shorter.

Conventional diesel combustion typically has a negative ignition dwell and therefore a significant quasi-steady period [2], where much of the heat release occurs through mixing-controlled combustion during the spray-driven diffusion flame phase. By contrast, for LTC conditions with positive ignition dwells, heat release does not overlap with the fuel injection event, so the quasi-steady jet is not an adequate model for combustion. Instead, as more mixing of air and fuel takes place prior to ignition, more of the heat release is premixed.

The evolution of the local equivalence ratios prior to combustion was investigated in a previous study [3] for a case of LTC combustion. The local fuel concentration within and between two neighboring jets was measured using planar laser-induced fluorescence (PLIF) of a fuel tracer (toluene) under non-reactive conditions. The three images presented in Fig. 1 show equivalence ratio contours corresponding to 12.7% intake oxygen concentration, which were derived from the fuel vapor concentration measurements under non-reacting conditions. The nozzle is located on the left side of the frames and the two studied jets are directed up and to the right and down and to the right of each image.

The first frame presents the results at the end of injection (EOI). The highest local equivalence ratios are located close to the nozzle, as for a quasi-steady jet. 2 crank angle degrees (CAD) after the end of injection (AEI), in the middle image, the mixtures are becoming leaner and close to stoichiometric in the upstream regions. The downstream regions are also becoming leaner but they are now richer relative to the near-nozzle region, which is contrary to the situation at EOI. This leaning trend continues in the bottom frame at 5 CAD AEI, where the mixture close to the nozzle is now below stoichiometric conditions. Formaldehyde imaging has shown that lean mixtures remain stagnant close to the nozzle late in the expansion stroke [4]. At equivalence ratios below 0.5, mixtures are unlikely to ignite or achieve complete combustion. Therefore, very lean mixtures in the near-nozzle region have been identified as potential sources of unburned hydrocarbons (UHC) emissions [3,4,5]. Also other studies have pointed out that over-lean mixtures could contribute to explaining the correlation between highly diluted LTC cases and engine-out UHC emissions [6,7,8].

The mixtures close to the nozzle shown in Fig. 1 become leaner very quickly after EOI. The air-entrainment rate in the jet after EOI can be compared to a steady jet case. The circled numbers in the top image represent the time needed in CAD for a fuel particle exiting the nozzle to reach the indicated locations in a steady-jet at the measured jet penetration rate. At the position of the second circle, the local equivalence-ratios are in the range 5 to 7. At the same location, i.e. 25 mm from the injector, the equivalence-ratios in the middle frame (2 AEI) are significantly lower, between 2 and 3. In the bottom image (5 AEI) mixtures become closer to stoichiometric in the downstream regions. These observations indicate a faster air-entrainment mechanism after the end of injection compared to a steady-jet.

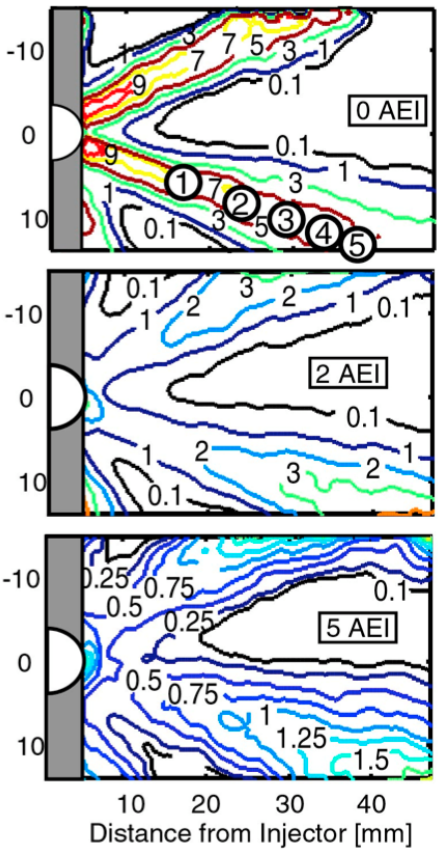

Figure 1 - Equivalence ratio contour lines for a portion of the combustion chamber obtained by fuel tracer fluorescence measurements [3]. The nozzle is located on the left side of the frames and two jets are directed up and to the right and down and to

the right in the image. The equivalence ratios correspond to 12.7% inlet oxygen. The circled numbers in the top image represent the time needed in CAD for a fuel particle exiting the nozzle to reach the indicated locations at the jet penetration rate.

Previous work also indicates that part of the UHC emissions during low-load LTC operations are caused by stagnant lean mixtures close to the injector after EOI [3]. The goal of this study is to investigate the potential to increase the upstream local equivalence ratios in the jet above the ignitability threshold by a post injection, and thereby reduce UHC emissions.

Toluene fluorescence is strongly affected by collisional quenching due to oxygen, so the technique is typically applied under non-reacting conditions. Non-reactive conditions can be seen as representative until ignition occurs. After ignition, combustion can significantly affect mixing. To investigate the effects of post-injections on the near-injector equivalence ratios and UHC emissions when ignition occurs near the post-injection event, it is more relevant to study reactive conditions. Therefore, the present investigation of post-injections uses other laser diagnostics for more indirect measurements of mixing.

Imaging of certain combustion intermediates can indicate the progression of two-stage ignition, and may even provide bounds on the local equivalence ratios. For example, Collin *et al.* used combined laser diagnostics to measure the distribution of OH and formaldehyde for HCCI combustion [9]. It was shown that formaldehyde is formed during the first-stage ignition and fills the measurement region in the studied case. When second-stage ignition occurs, OH is detected in small pockets within the formaldehyde region without overlapping. As second-stage ignition continues, OH regions grow and merge while formaldehyde regions are consumed. Therefore, OH- and formaldehyde-PLIF can indicate the ignition-stage that a region of interest goes through.

Similar combined laser diagnostics were employed by Genzale *et al*. on LTC combustion [7]. Observations of the OH and formaldehyde distributions relative to the first- or second-stage ignition were similar to the ones reported previously. Furthermore, toluene-PLIF was used under non-combusting conditions to obtain quantitative information about local equivalence ratios. The comparison between LIF images of OH, formaldehyde, and PAH under reacting conditions with and toluene fluorescence under non-reacting conditions showed how the spatial distribution and temporal evolution of the combustion intermediates can provide boundaries on the local equivalence ratio. Firstly, formaldehyde first appears in regions ranging from from fuel-lean to fuel rich, but it persists late in the cycle only in fuel-lean regions, for which the delay to second-stage ignition is very long. Second, OH concentrations are highest in regions of intermediate stoichiometry, and the OH fluorescence signal should be roughly proportional to its concentration [10], so that OH fluorescence during its initial appearance is strongest in regions that are likely of intermediate stoichiometry. Finally, PAH fluorescence arises in regions that are fuel-rich and later may proceed to soot formation.

In a similar manner, combustion intermediates are used as quantitative indicators of local stoichiometry in the present investigation. Two different post-injection strategies are presented and compared to a single injection in terms of engine-out UHC level, and estimated distributions of near-stoichiometric, lean and potentially rich mixtures derived from laser-induced fluorescence imaging of OH and formaldehyde/PAH. One of the injection strategies is shown to rapidly render the mixture in the upstream regions combustible and thereby decrease UHC emissions by 20% at the same load as a single injection condition. Rate of injection measurements and sensitivity of the post-injection parameters on UHC reduction are also discussed.

EXPERIMENTAL SETUP AND DIAGNOSTICS

OPTICAL ENGINE

The optical engine is a single cylinder version of a Cummins N-series heavy-duty diesel engine having a bore of 139.7 mm, a displacement of 2.34 liters, and a swirl ratio of 0.5. Other specifications are listed in Table 1. Figure 3 is a schematic showing the extended Bowditch piston with a large flat piston-crown window, small rectangular windows located at the top of the cylinder liner providing cross-optical access for laser-based diagnostics. It has also a small cylinder head window in place of one of the exhaust valves. The piston bowl-rim has a cut-out to allow laser-sheet access to the combustion bowl near top dead center (TDC), see Fig. 2. More details about the optical engine can be found in [2,11,12].

The engine is equipped with a Cummins XPI high-pressure, electronically controlled common-rail fuel injector. This injector uses a solenoid-actuated pilot valve and a pressure-balanced needle to control fuel delivery. It is capable of multiple injections at up to 2000 bar fuel-rail pressure. For the experiments presented here, an eight-hole mini-sac injector cup (tip) was employed, having an included angle of 152°. The eight orifices are equally spaced and have a nominal diameter of 0.15 mm.

Table 1 Engine and injector specifications.

Engine base type	Cummins N-14, DI diesel
Number of cylinders	1
Cycle	4-stroke
Number of intake valves	2
Number of exhaust valves	1*
Combustion chamber	Quiescent, direct injection
Swirl ratio	0.5 (approx.)
Bore	139.7 mm
Stroke	152.4 mm
Bowl width	97.8 mm
Displacement	2.34 liters
Connecting rod length	304.8 mm
Piston pin offset	None
Geometric compression ratio	11.2:1
Simulated compression ratio	16:1
Fuel injector type	Common-rail, solenoid actuated
Cup type	Mini-sac
Number of hole	8, equally spaced
Spray pattern included angle	152°
Rail pressure	1600 bar
Orifice treatment	None (square edged)
Nominal orifice diameter	0.15 mm

*In this optically accessible diesel engine, one of the two exhaust valves of the production cylinder head was replaced by a window and periscope.

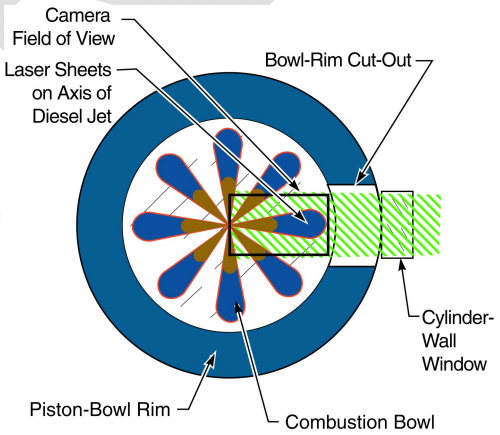

Figure 2 – Schematic of the piston with eight-hole injector. The laser sheets enter the combustion chamber from the right side through a cut-out in the bowl rim and follow the jet axis towards the injector nozzle.

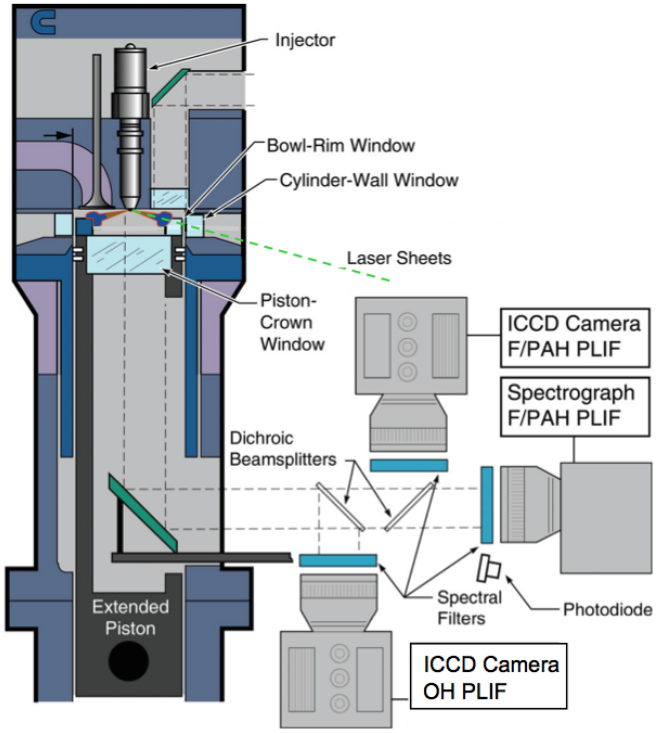

Figure 3 - Schematic of the optical heavy-duty diesel engine and layout for the combined laser induced diagnostics.

OPERATING CONDITIONS

The engine operating conditions are summarized in Table 2. To achieve LTC conditions, the oxygen concentration was reduced to 12.7% in the inlet flow. Because the engine is a single-cylinder, and skip-fired for thermal loading reasons, EGR was not available for dilution. Rather, a metered flow of nitrogen was added to the intake stream to dilute the oxygen concentration to the desired level. At the chosen dilution of 12.7% O_2, the adiabatic flame temperature for a stoichiometric mixture at peak pressure is 2170 K, compared to 2680 K for pure air. Ojeda *et al.* have shown that this level of dilution can comply with the NO_X limit of the US 2010 heavy-duty on-road legislation without NO_X after-treatment for a wide load range by adjusting the injection strategy [13].

The injection parameters are given for the different injection strategies in Table 3. The values for actual start and duration of injection are extracted from injection rate measurements for each strategy. The fuel mass delivered in the post-injection is discussed together with rate of injection results in a later section.

Table 2 Engine operating conditions.

Engine speed	1200 rpm
Engine load	280 kPa IMEPg
Intake O_2	12.7%
Common-rail fuel pressure	1600 bar
TDC Motored Density	22.1 kg/m^3
TDC Motored Temperature	837 K
TDC Motored Pressure	54.9 bar
Intake Pressure	214 kPa (abs)
Intake Temperature	78°C

Table 3 Injection parameters for the different strategies.

	Single Main Injection	Main + Small Post Injection	Main + Large Post Injection
Actual Start of Main Injection	-5° ATDC	-5° ATDC	-5°ATDC
Actual Duration of Main	~980 μs	~970 μs	~830 μs
Actual Start of Post Injection	-	3°ATDC	4°ATDC
Actual Duration of Post Injection	-	~200 μs	~560 μs
Total Fuel Injected	39.2 mg	41 mg	44.7 mg

For all operating conditions, cylinder pressure and fuel rail pressure were digitized and recorded at quarter CAD increments, simultaneously with the acquisition of the optical data. The apparent heat release rate (AHRR) was calculated from ensemble-averaged pressure data using an air-standard first-law analysis (see e.g. [14]). A regular schedule is maintained during these experiments where the engine is motored for 90 seconds before the injecting fuel to minimize variability of results due to transients.

A diesel primary-reference fuel (PRF) mixture was used to avoid unwanted fluorescence interferences from aromatic components in diesel fuel. The PRF mixture is 32.3% n-hexadecane (cetane) and 67.7% heptamethylnonane by volume, giving a defined cetane number of 42.5, which is typical of U.S. diesel fuel [15].

Rate of injection analysis

Multiple injection strategies can possibly affect the dynamics in the injector due to pressure waves in the common rail system. To understand the effects of pressure waves on post injections, the rates of injection for the strategies in Table 3 were measured using a spray-impingement meter [16]. Fig. 4 shows the derived mass rate of injection for all three cases. The rail pressure in the fuel line upstream of the injector is also indicated on the plot. Both parameters are averaged over 100 injections and low-pass filtered using a Butterworth filter with a normalized cutoff frequency of 0.1. The rate of injection was measured with atmospheric back-pressure and the nozzle was heated to 90°C, which corresponds to the nominal temperature of the coolant in the engine cylinder head. The low pressure of the injector test chamber compared to the in-cylinder pressure close to TDC could influence the injection rate measurements. The spray velocity is proportional to the square root value of the pressure difference between the nozzle-sac and the surrounding air. However, Klein-Dowel *et al.* showed that for fully cavitating flows in similar injectors, the mass flow rate was independent of the chamber pressure [17]. Cavitating flow is estimated to occur above 200 bar injection pressure.

It appears clearly on the figure that the delayed post-injection strategy, i.e. actual start of post injection at 4°ATDC, shows a much larger fuel mass in the post-injection compared to the strategy with an earlier post-injection at 3°ATDC. It is important to note that both post-injection strategies had the same energizing time from the injector control system. The two strategies only differ by a delay of 1 CAD in the start of injection command. The main injection duration was reduced in the large post-injection strategy to maintain roughly constant load with the increased post-injected fuel mass. The start of the main-injection was kept unchanged. The results gave 39.2 mg of fuel per injection with a standard deviation of 0.9 mg for the single injection only and 41.0 mg for the main and small post-injection together. The large post-injection strategy resulted in 44.7 mg of fuel per cycle. Analysis of the rate of injection results shows that 14.6 mg of the 44.7 mg are injected in the large post injection with a standard deviation of 0.6 mg. On the other hand, only 1.8 mg of 41.0 mg are post-injected in the small post-injection strategy. The standard deviation for this post injection is 0.4 mg. These values are determined from 100 cycles.

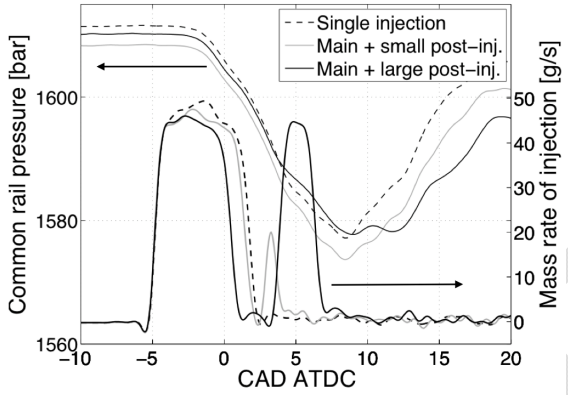

Figure 4 – Rate of injection for all three injection-strategies averaged over 100 cycles and low-pass filtered. The fuel pressure in the common rail is also indicated.

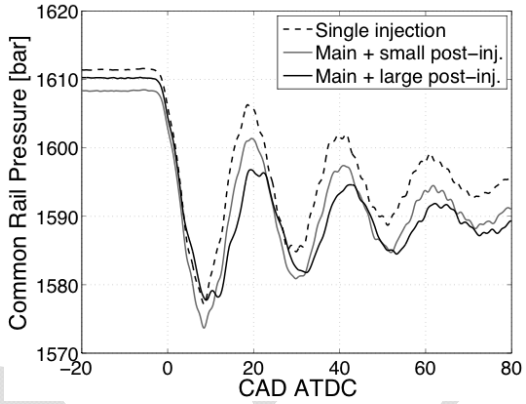

Figure 5– Fuel pressure oscillation in the common rail due to pressure waves in the fuel lines after the different injection strategies.

The mass of post-injected fuel in the small post-injection strategy appears to be very small. However, repeatability tests in the engine and the rather low standard deviation obtained for the post-injected fuel mass indicate that such a small post-injection is achievable.

A reasonable explanation for the large difference in post-injected fuel-mass despite an identical energizing time could be the presence of pressure waves in the high-pressure fuel system generated by the main injection. The change in timing of the post-injection changes the opening time for the injector needle relative to the pressure waves and could cause a variation in the actual injection duration and injected fuel mass.

The fuel pressure before the injector was monitored by a Kistler pressure transducer in the common rail. Fig. 5 shows the fuel pressure in the common rail for the different injection strategies. Significant variations are observed after the main injection. However, the common rail pressure data is also presented in Fig. 4 together with the injection rate data for direct comparison. It appears that the timescale between the main and post-injections is smaller than the dynamics of the fuel system. For both post-injection strategies, SOI for the post-injections is occurring at comparable fuel pressure conditions. Nevertheless, injector and fuel line dynamics are very complex and the conditions depicted at the location of the pressure transducer may be very different from the ones at the nozzle. (Pressure waves within the injector body are very likely to play a role in the opening of the needle as well.)

LASER DIAGNOSTICS

The objective of this investigation is to qualitatively observe the effects of post-injected fuel in the over-mixed near-nozzle region. Two effectively simultaneous planar laser-diagnostics were used to investigate species that mark the progress of a two-stage

autoignition process, as well as to provide an indication of mixture stoichiometry (i.e. lean, rich, or intermediate stoichiometry) at their location along the centerline of one of the eight jets. PLIF of OH was employed to identify the regions that have achieved second-stage ignition and to provide an indicator of mixtures that are of intermediate stoichiometry [10]. PLIF at 355 nm was imaged both with a camera and a spectrometer. By spectrally analyzing this fluorescence, the locations of formaldehyde and PAH could be determined. Regions with PAH fluorescence indicate fuel-rich mixtures, while regions with persistent formaldehyde fluorescence late in the cycle indicate fuel-lean mixtures [7].

OH fluorescence (OH-PLIF) was excited near 284 nm using 20 mJ per pulse provided by the frequency-doubled output of an optical parametric oscillator (OPO) pumped by the 355-nm third-harmonic of a Nd:YAG laser. A 105mm UV-Nikkor lens was mounted on a UV camera to collect the fluorescence emission. The positions of the cameras are shown in Fig. 3. To maximize the signal/noise ratio and reject elastic-scattered laser light, several filters were employed. Since OH-fluorescence is narrow-band, a 16nm wide bandpass filter centered at 310 nm was used. A 2-mm thick WG 305 long-wave-pass filter was employed to remove the scattered laser light at 284 nm. Finally, a 358-nm short-pass filter rejected fluorescence from other species and other interference such as black body radiation from soot. Further information about OH-PLIF can be found in [18].

Both formaldehyde and PAH fluorescence (formaldehyde/PAH PLIF) were excited simultaneously by a single 355-nm beam of a frequency-tripled Nd:YAG laser at 60 mJ per pulse. The resulting combination of formaldehyde and PAH fluorescence was imaged by a second camera (see Fig. 3). A CG385 long-pass filter removed the scattered laser-light while a 40-nm wide bandpass filter centered at 408 nm isolated the fluorescence signal of interest from other species. To distinguish formaldehyde fluorescence from that of PAH in the images, the fluorescence emission was spectrally analyzed to discriminate the signatures of formaldehyde and PAH in the total signal. A beam splitter directed part of the fluorescence emission along the jet axis onto the entrance slit of an Oriel 1/8-meter spectrometer using a 55-mm f/2.5 glass lens, as shown in Fig. 2. A CG375 long-pass colored glass filter was placed in front of the lens to help reject strong elastic scatter from the laser. The fluorescence spectrum was imaged onto an intensified CCD array at the exit of the spectrograph, capturing emission from 380 nm to 450 nm. An Oriel 77298 grating with 1200 lines/mm blazed at 350 nm and a slit opening of 600 μm gave a resolution of 4 nm.

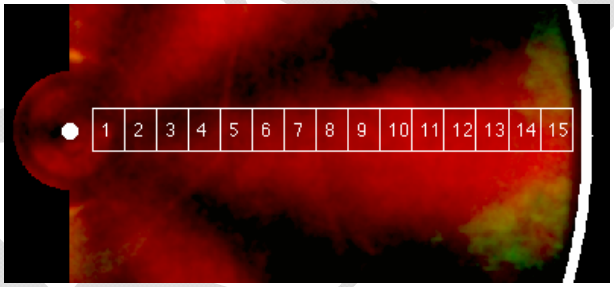

Figure 6 – Visualization of the binning zones used for the spectral evaluation of the formaldehyde/PAH LIF along the jet axis.

The region of the combustion chamber viewed by the spectrograph is a 4.2-mm wide band along the jet axis. As illustrated in Fig. 6, this narrow band was divided into 15 discrete zones in the axial direction. In each zone, the signal captured with the spectrometer was compared to a reference formaldehyde-spectrum. The reference spectrum was extracted from the acquired combustion-spectra at a timing and location dominated by premixed burn. The premixed phase of the combustion is characterized by the presence of formaldehyde. Spectra from different binning zones are presented as examples in Fig. 7 together with a formaldehyde reference-spectrum.

A typical feature of the formaldehyde spectrum is its regular peak spacing. Seven characteristic peaks between 385 and 445 nm can be considered as its fingerprint. In noisy spectra, a bandpass filter can thereby distinguish potential formaldehyde peaks from more broadband features. Fig. 8 presents the signal in Fig. 7 after bandpass filtering. The spectral peaks appear clearly in the reference spectrum and the similarity or non-similarity of the reference signal from the signal integrated within each measurement zone becomes more obvious.

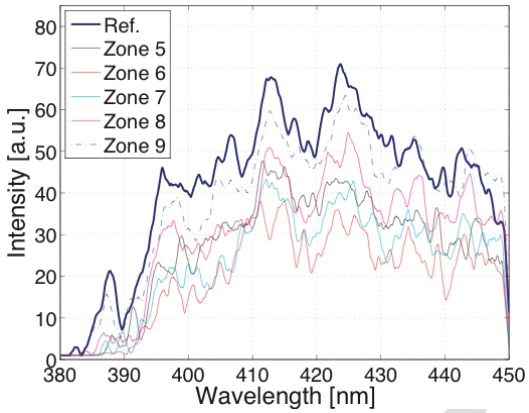

Figure 7 – Example of spectral visualization of the formaldehyde/PAH LIF signal for several binning zones. A reference spectrum is plotted for comparison.

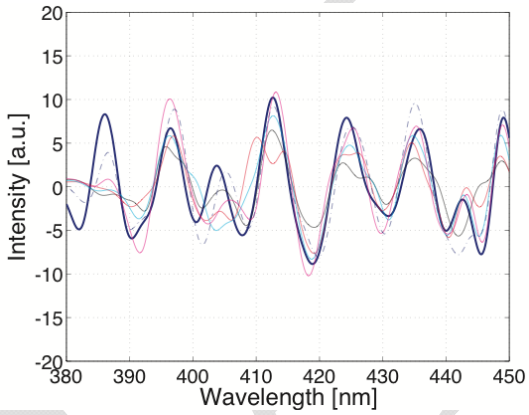

Figure 8 – Bandpass-filtered spectra for the binning zones presented in Fig. 7

The spectra are compared using the normalized covariance of the two signals for each zone, similarly to the approach in [19]. The correlation value obtained is between zero (i.e. no correlation to the reference spectrum) and unity (i.e. perfect correlation). The correlation value is visually represented in a color bar placed under the studied spray, see Fig. 9. The bar is divided into 15 zones and the color of each zone reflects the similitude of the fluorescence signal to formaldehyde along the jet axis, with black indicating zero and red indicating unity.

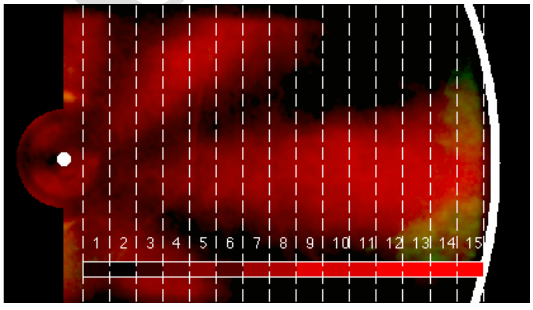

Figure 9 – Image resulting from the spectral analysis. The darkest colors in the correlation bar indicate a low correlation with a formaldehyde reference spectrum whereas the brightest color indicate that the LIF signal has a high probability of being formaldehyde-LIF signal.

RESULTS

UHC EMISSIONS FOR LTC CASES

As discussed earlier, EGR-diluted LTC conditions have low combustion temperatures for limiting NOx formation, and they typically have a positive ignition dwell. This is necessary to increase pre-combustion mixing and thereby limit the formation of soot during combustion. Both the ignition dwell, which creates locally lean mixtures, and the lower combustion temperature contribute to UHC emissions. Higher load conditions have longer injection durations and therefore shorter ignition dwells, as well as somewhat higher in-cylinder temperatures because of compression-heating from the rise in pressure from the combustion event. Consequently, UHC emissions are a strong function of load.

Figure 10 shows how the load-specific UHC emissions decrease with increasing gross indicated mean effective pressure ($IMEP_g$) for a load sweep for the single-injection condition in our engine. Only the duration of the main injection was changed during the load sweep, and UHC data are adjusted to account for skip-fired operation mode (the data correspond to continuously-fired operation). The exhaust gases were analyzed with a 600 HFID flame ionization analyzer from California Analytical Instruments. A heated line sampled gas from the exhaust pipe as close as possible to the engine, approximately 20 cm from the exhaust port, to avoid effects of potential condensation of heavier hydrocarbons in the exhaust pipe before the sampling point. Heat insulation material was employed on the exhaust and sampling pipe to further avoid condensation issues of the exhaust gases. For this study, we selected a target load at 280 kPa $IMEP_g$ for comparison of single-injection with post-injection UHC emissions performance. The specifications of the injection strategies are given in Table 3.

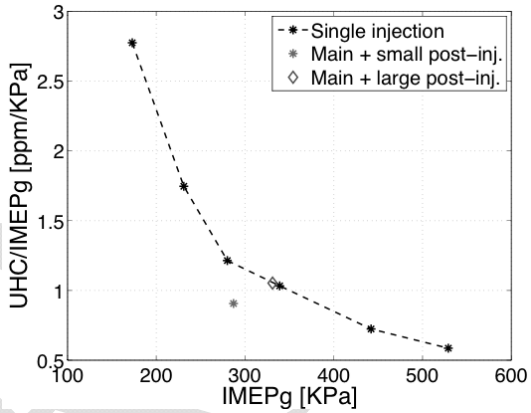

Figure 10 – Engine-out UHC measurements versus $IMEP_g$ for LTC cases. The result for the investigated post-injection strategy is indicated. The UHC levels presented are corrected for skip-fired operation mode.

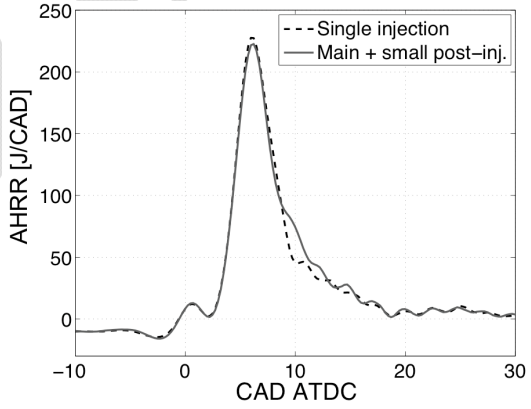

Figure 11 –Apparent rate of heat-release for the main-injection only compared to the investigated post-injection strategy leading to exhaust UHC reduction while keeping the load constant.

The post-injection condition reported in the next sections shows a 20% reduction in UHC emissions at the same load as the reference case with main injection only. The UHC emissions results for this post-injection strategy are presented in Fig. 10 for direct comparison with the single-injection cases. The apparent heat release rate for both injection strategies is presented in Fig. 11. The start of main injection is identical for both strategies, and the injection duration for the main-only strategy is slightly longer. Therefore, the heat release rate is very similar for both cases regarding the cool flame and the start of combustion. The actual start of the post-injection occurs close to 3 CAD ATDC. The small difference in peak value between the two curves can be explained by the higher fuel mass in the main injection for the single-injection case, as well as the reduction of apparent heat release due to evaporation of the post-injected fuel near the timing of the peak. The evidence of the combustion of the post injection is visible between 9 and 12 CAD ATDC. Thereafter the two curves merge through the end of the combustion event. The fuel mass injected in the post-injection was kept as low as possible. The energizing time employed for the second injection was set as the shortest duration assuring a reasonable cycle-to-cycle repeatability of the injection quantity. Rate-of-injection measurements for the different injection strategies show that a very short (approximately 200 microsecond) post-injection is achieved, as discussed in an earlier section.

LASER DIAGNOSTICS RESULTS

Single injection

The laser diagnostic results presented in Fig. A1 (in the appendix section) show combined images of OH-PLIF (false-colored green) and formaldehyde/PAH-PLIF (red) for the single main injection condition. The data are averaged over twelve separate cycles for a better signal to noise ratio given the rather low cycle to cycle variations in the observed phenomena. The nozzle is located on the left side of the images and the jet of interest is penetrating horizontally from left to right. The bowl wall is indicated in the frames, but it should be noted that a wall cut-out was present at the studied jet to enable laser sheet access, see Fig. 2.

The end of the single injection is visible in the first frame by scattered light from the liquid portion of the jet. The signal is not revealing the presence of OH-radicals in this region since offline images show the same scattered light pattern. Offline images are taken when the laser wavelength is tuned away from the OH excitation lines. The intensity of the scattered light in the liquid spray is lower for the studied jet compared to the neighboring ones. Attenuation of the laser intensity after intersecting with the jet is a plausible explanation for low scattering signal from the horizontal fuel spray.

The formaldehyde/PAH-PLIF signal appears in a jet shape already by EOI. The jet structure is clear and remains for 8 CAD after EOI. The formaldehyde correlation level along the centerline of the jet indicates that the signal in the downstream portion of the jet is highly correlated with the formaldehyde reference spectra. The jet is progressively filled with formaldehyde towards the upstream regions in the following frames.

By five CAD after EOI, OH-LIF signal is detected in the vicinity of the bowl wall. It indicates progression to second-stage ignition and relatively complete combustion in mixtures of intermediate stoichiometry, between fuel-lean and fuel-rich [10]. The regions of OH-fluorescence progress toward the nozzle (to the left) for a short period (6 CAD), after which the fluorescence decreases in intensity.

Formaldehyde fluorescence remains in the region between the nozzle and halfway to the bowl wall throughout the entire combustion event. The presence of formaldehyde indicates regions of partially oxidized fuel that have not yet achieved second-stage ignition. The downstream regions of OH fluorescence do not propagate upstream to the near injector region, indicating that the region of formaldehyde fluorescence late in the cycle is a source of UHC emissions. This observation agrees with previous studies [3,4,5] that showed the presence of unburned fuel remaining close to the nozzle due to over-leaning after EOI. Although many possible sources of engine-out UHC exist, such as unburned fuel in the crevices [20], flame quenching at the wall [14] or injector dribble [21] for example, the near-nozzle region is of major interest in the present study.

Small post-injection strategy leading to lowered UHC emissions

The post-injection strategy investigated in this section was previously shown to yield 20% lower engine-out UHC emissions as compared to using only a single injection at the same load (Fig. 10). The laser diagnostic results are presented in Fig. A2 in a similar outline as the single injection case. The scattered light on the liquid part of the jets reveals the end of the main injection by one CAD after TDC. After a one-degree dwell, the post-injection starts. Given the short exposure time of the frames, it can be concluded that the actual duration of the post injection is between one and two CAD (140-280 microseconds), which is consistent with the rate of injection measurements (~200 microseconds).

The initial development of combustion, in terms of formaldehyde and OH-radicals, is similar to the single-injection case previously described. The horizontal jet fills with formaldehyde a few CAD after the end of the main injection and OH is formed in the downstream regions. However, ten degrees after the main EOI (11 ATDC), OH radicals are rapidly formed in the upstream part of the jet, within the field of formaldehyde fluorescence. The following frames show that OH-radicals continue to progressively fill the jet cross-section and propagate upstream. By 10 CAD after the end of the post-injection (14 ATDC), OH radicals are found in the near-nozzle region where only formaldehyde was detected with the single injection. Afterward, the OH signal weakens, and the strongest intensities generally remain downstream. The spatial development of the OH distribution along the jet axis is illustrated in Fig. 12. A threshold intensity of 10 out of the full-scale value of 255 is used to determine the downstream distance of OH from the OH-PLIF images.

The appearance of OH fluorescence in the near-injector regions formerly occupied by formaldehyde implies that the post injection has helped to raise the local equivalence ratio from fuel-lean to more intermediate stoichiometry. The flammable mixture ignites rapidly in the jet and second stage ignition reaches the near-nozzle region. The present diagnostics do not quantify the effect of the post-injection on upstream UHCs. However, the observation of the increased upstream OH fluorescence together with the exhaust-gas measurements strongly suggest that a significant part of the near-injector UHC were oxidized as a consequence of the post-injection. Significant formaldehyde fluorescence still remains late in the cycle, however, indicating that the small post injection investigated here does not entirely consume the unburned fuel near the injector.

Finally, there are no clear signs of PAH in the 355-nm PLIF data. Therefore, the post-injection is not suspected to create fuel-rich soot-forming zones in the wake of the main injection.

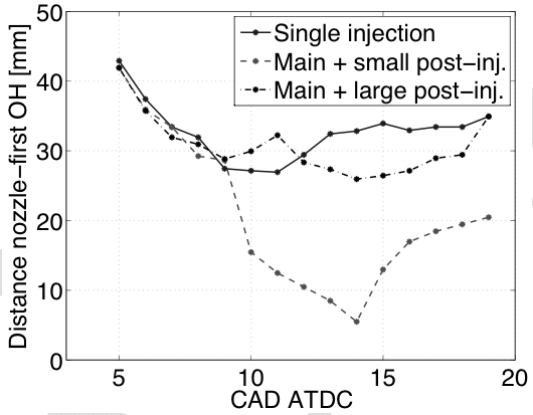

Figure 12 - Evolution of the OH-radicals downstream position relatively to the injector nozzle in the jet-axis plane for the single-injection compared to both the investigated post-injection strategies.

Large post-injection strategy leading to unchanged UHC emissions

The small post-injection strategy described in the previous sections, which yields a 20% reduction in UHC emissions, was quite unique, and was discovered by trial and error. In fact, most of the post-injection strategies that we investigated in our parameter sweeps produced little or no reduction of UHC emissions, or even increased UHC emissions at the same load. This section presents one example of an alternative post-injection strategy that does not yield a reduction of UHC emissions. Comparison of this alternative condition with the more optimized post-injection strategy helps to illustrate the sensitivity of the post-injection timing and quantity on UHC emissions as well as to better understand the underlying mechanism. In the alternative strategy, the post-injection was delayed by one CAD compared to the case previously discussed. Because of fuel rail and possibly injector dynamics, the delay caused the post-injection quantity to be increased, even though the command duration was held constant. To offset the increased mass in the post injection so that load could be held constant, the injector solenoid energizing time of the main injection was decreased, while the start of the main injection was kept unchanged.

The exhaust-gas measurements revealed that this large post-injection strategy had no significant effect on UHC emissions compared to a single injection at the same load. The laser diagnostic data for the large post-injection strategy are presented in Fig. A3. Prior to 8 CAD after the main EOI (9 ATDC), the formaldehyde and OH distributions are generally the same as for the other injection strategies. However, scattered light from the liquid sprays reveals a significantly longer post-injection duration than the previous post-injection strategy.

Then, between 10 and 12 CAD after the main EOI, strong formaldehyde/PAH-PLIF signal is visible in the downstream region of the jet. It is reasonable to assume that the post-injected fuel is at the origin of this observation since the region was filled with OH radicals prior to that timing. In the image at 12 CAD ATDC, the formaldehyde correlation coefficient is low in the downstream regions along the jet centerline. It indicates a probable presence of PAH due to locally richer mixtures caused by the large post-injection, which was not observed with the single main injection.

During the same period, the evolution of the OH distribution is different from the small post-injection case. Here, second-stage ignition is not observed in the upstream regions close to the injector. It progresses only slightly upstream, staying in the outer portion of the bowl wall. Late in the cycle, the formaldehyde and OH signals remain separated, with formaldehyde close to the injector and OH close to the bowl wall, with a decreasing intensity in time. This indicates that the mixtures in the upstream regions did not go through second-stage ignition despite the use of a post-injection.

Importance of post-injection momentum flux for UHC reductions

Based on the observed differences in the evolution of formaldehyde and OH between the single injection case and the small and large post-injection strategies, the momentum of the post-injection appears to affect the mechanism for UHC reduction close to the nozzle. With a single injection with a relatively large total momentum, the front of the jet penetrates to the bowl wall, while the upstream wake over-mixes. The upstream mixtures become too fuel-lean to achieve second-stage ignition, so that formaldehyde and UHCs persist late in the cycle. Similarly, for the large post injection, the formaldehyde fluorescence intensity increases at 9 CAD after the main EOI (10 ATDC), and the post-injection jet penetrates toward the bowl wall, pushing the residual OH from the main injection farther downstream. This observation is clear in Fig. 12 where the distance between the nozzle and the first OH signal on the jet axis is compared for all three cases. The downstream movement of OH for the large post injection is apparent in Fig. 12 between 9 and 10 CAD after the main EOI (10-11 ATDC). Additionally, the upstream wake for the large post injection shows formaldehyde persisting late in the cycle, indicating overly lean mixtures and incomplete combustion, similar to the single injection. Later in the cycle, the OH radicals do not interact with the upstream non-oxidized fuel, which explains the results of unchanged exhaust gas UHC content.

For the small post injection, however, the post-injection jet does not displace the OH downstream, so it does not appear to have penetrated to the wall at ignition. Instead, the upstream mixtures achieve second-stage ignition indicated by the upstream appearance of OH, as illustrated in Fig. 12. The upstream appearance of OH strongly suggests that upstream mixtures have been enriched by the small post injection so that chemical kinetics leading to second-stage ignition are accelerated. The low momentum of the small post-injection likely contributes to its ability to enrich the near-injector region without penetrating so far downstream and leaving fuel-lean mixtures in its wake.

The momentum flux in the jet is proportional to the product of the mass flow rate and the outlet velocity. The rate of injection results in Fig. 4 show that the mass flow through the nozzle holes is approximately doubled in the large post-injection compared to the previous one. As a consequence, the momentum is also significantly larger, approximately 14.7 $g.m.s^{-1}$ compared to 1.3 $g.m.s^{-1}$ for the small post-injection. Therefore, for the operating conditions examined here, the post-injection momentum threshold to achieve UHC reduction is apparently somewhere between 1.3 and 14.7 $g.m.s^{-1}$.

SUMMARY/CONCLUSIONS

For diesel LTC, overleaning in the jet during the ignition dwell has previously been identified as a potential source of UHC. The ignition kinetics are too slow in the fuel-lean near-injector regions for combustion to proceed to second-stage ignition and complete combustion in the time available. The present study investigated the potential of a post-injection strategy to enrich the near-injector regions with additional fuel, and thereby hasten the ignition chemistry so that more complete combustion would be achieved and UHC emissions would be reduced. In addition to exhaust-gas UHC measurements, combined laser-diagnostics were employed to identify fuel lean, near stoichiometric, and fuel rich regions along the jet path. The following conclusions can be drawn from the study:

- A post-injection strategy was identified that effectively reduced engine-out UHC emissions by 20% compared to a single injection at the same load.

- For the single-injection condition, PLIF measurements at 355 nm showed formaldehyde fluorescence in the near-injector region late in the cycle, which is indicative of overly fuel-lean mixtures that do not achieve complete combustion. Images of OH-PLIF confirmed that second-stage ignition only occurs farther downstream in the jet where mixtures are likely of more intermediate stoichiometries

- For a small post-injection condition, the energizing time was set to the shortest duration assuring a lift of the injector needle at every cycle. OH-PLIF measurements revealed second-stage ignition occurring in the upstream region of the jet within a few CAD after the post-injection. The post-injection is thereby capable of enriching the local mixtures near the injector so that the chemical kinetics become fast enough to achieve more complete combustion in the time available.

- For an alternative strategy with a smaller main injection and a larger post injection, OH fluorescence did not indicate second-stage ignition occurring in the upstream regions. This observation suggests that the momentum delivered in the post-injection needs to be low so that the penetration is relatively short. Thus, the post-injected fuel remains in the near-injector region to enrich the over-mixed zones that lead to UHC emissions, and is not carried too far downstream by the post-injection momentum.

REFERENCES

1. Kook, S., Bae, C., Miles, P.C., Choi, D., and Pickett, L.M, "The Influence of Charge Dilution and Injection Timing on Low-Temperature Diesel Combustion and Emissions," SAE paper 2005-01-3837, 2005.

2. Dec, J.E., "A Conceptual Model of D.I. Diesel Combustion Based on Laser-Sheet Imaging," SAE Paper 970873, SAE Transactions, 106, No. 3, pp. 1319-1348, 1997.

3. Musculus, M. P. B., Lachaux, T., Pickett, L. M., and Idicheria, C. A., "End-of-Injection Over-Mixing and Unburned Hydrocarbon Emissions in Low- Temperature-Combustion Diesel Engines," SAE Paper 2007-01-0907, SAE Transactions, 116, No. 3, pp. 515-541, 2007.

4. Lachaux,T. and Musculus, M.P.B., "In-cylinder Unburned Hydrocarbon Visualization during Low-Temperature Compression-Ignition Engine Combustion Using Formaldehyde PLIF," Proc.Combustion.Inst.,2007.

5. Kim, D., Ekoto, I., Colban, W.F. and Miles, P.C., "In-cylinder CO and UHC Imaging in a Light-Duty Engine Diesel Engine during PPCI Low-Temperature Combustion," SAE paper 2008-01-1602, 2008.

6. Han, M. Assanis, D.N. and Bohac, S.V., "Sources of Hydrocarbon Emissions from Low-Temperature Premixed Compression Ignition Combustion from a Common Rail Direct Injection Diesel Engine", Combustion Science and Technology, 181: 3, pp. 496-517, 2009.

7. Genzale, C.L., Reitz, R.D., and Musculus, M.P.B., "Effects of Jet-Bowl and Jet-Jet Interactions on Late-Injection Low-Temperature Heavy-Duty Diesel Combustion", Proceedings Thiesel 2008, 2008.

8. Koci, C.P., "Detailed Unburned Hydrocarbon Investigations in a Highly-Dilute Diesel Low Temperature Combustion Regime," SAE paper 2009-01-0928, 2009.

9. Collin, R., Nygren, J., Richter, M., Aldén, M., Hildingsson, L., Johansson, B., "Simultaneous OH- and Formaldehyde-LIF Measurements in an HCCI Engine," SAE paper 2003-01-3218, 2003.

10. Singh, S., Musculus, M.P.B and Reitz, R.D, "Mixing and flame structures inferred from OH-PLIF for conventional and low-temperature diesel engine combustion," Combustion and Flame 156 (2009), pp. 1898-1908, 2009.

11. Musculus, M. P. B., Dec, J.E. and Tree, D. R., "Effects of Fuel Parameters and Diffusion Flame Lift- Off on Soot Formation in a Heavy-Duty Diesel Engine," SAE Paper 2002-01-0889, SAE Transactions, Vol. 111, No. 3, 1467-1489, 2002.

12. Espey, C. and Dec, J.E., "Diesel Engine Combustion Studies in a Newly Designed Optical Access Engine Using High-Speed Visualization and 2-D Laser Imaging". SAE paper 930971, SAE Trans. 99 (4), pp 703-723, 1993.

13. Ojeda W., Zoldak P., Espinosa R., and Kumar R., "Development of a Fuel Injection Strategy for Partially Premixed Compression Ignition Combustion", SAE Paper 2009-01-1527, SAE International Journal of Engines 2(1), 1473-1488, 2009.

14. Heywood, J. B., Internal Combustion Engine Fundamentals, McGraw-Hill, Inc., 1988.

15. Bobba, M.K, Chartier, C., Andersson, Ö., Johansson, B., Musculus, M.P.B, “Planar Laser-Diagnostics of Soot and OH with Post-Injections in a Heavy-Duty LTC Diesel Engine”, Proceedings Thiesel 2010, 2010.

16. Musculus, M. P. B., "On the Correlation between NOx Emissions and the Diesel Premixed Burn," SAE Paper 2004-01-1401, SAE Transactions, Vol. 113, No. 4, 631-651, 2004.

17. Klein-Douwel, R. J. H., Frijters, P. J. M., Seykens, X. L. J., Somers, L. M. T. and Baert, R. S. G. “Gas Density and Rail Pressure Effects on Diesel Spray Growth from a Heavy-Duty Common Rail Injector,” Energy & Fuels 2009, 23, pp. 1832–1842, 2009.

18. Kohse-Höinghaus, K. “Laser techniques for the quantitative detection of reactive intermediates in combustion systems”. Progress in Energy and Combustion Science, 20, 203-279, 1994.

19. Genzale, C.L., Reitz, R.D. and Musculus, M.P.B. “Effects of Piston Bowl Geometry on Mixture Development and Late- Injection Low-Temperature Combustion in a Heavy-Duty Diesel Engine,” SAE paper 2008-01-1330, 2008.

20. Aceves, S.A., Flowers, D.L., Espinosa-Loza, F., Martinez-Frias, J., Dibble, R.W., Christenson, M., Bengt, J., and Hessel, R.P., "Piston-liner crevice geometry effect on HCCI combustion by multi-zone analysis," SAE Paper 2002-01-2869, SAE Transactions, 111, 2002.

21. Greeves, G., Khan, I. M., W ang, C.H.T., and Fenne, I., "Origins of Hydrocarbon Emissions from Diesel Engines," SAE Paper 770259, SAE Transactions, 86, 1977.

AKNOWLEDGMENT

The optical engine experiments were performed at the Combustion Research Facility, Sandia National Laboratories, Livermore, CA. Support for this research was provided by the U.S. Department of Energy, Office of Vehicle Technologies and the Swedish Energy Agency. Sandia is a multi-program laboratory operated by Sandia Corporation, a Lockheed Martin Company for the United States Department of Energy’s National Nuclear Security Administration under contract DE-AC04-94AL85000. The authors express their gratitude to David Cicone and Chris Carlen of Sandia National Laboratories for their great assistance and dedication with maintaining the research engine and the lasers used in these experiments.

APPENDIX

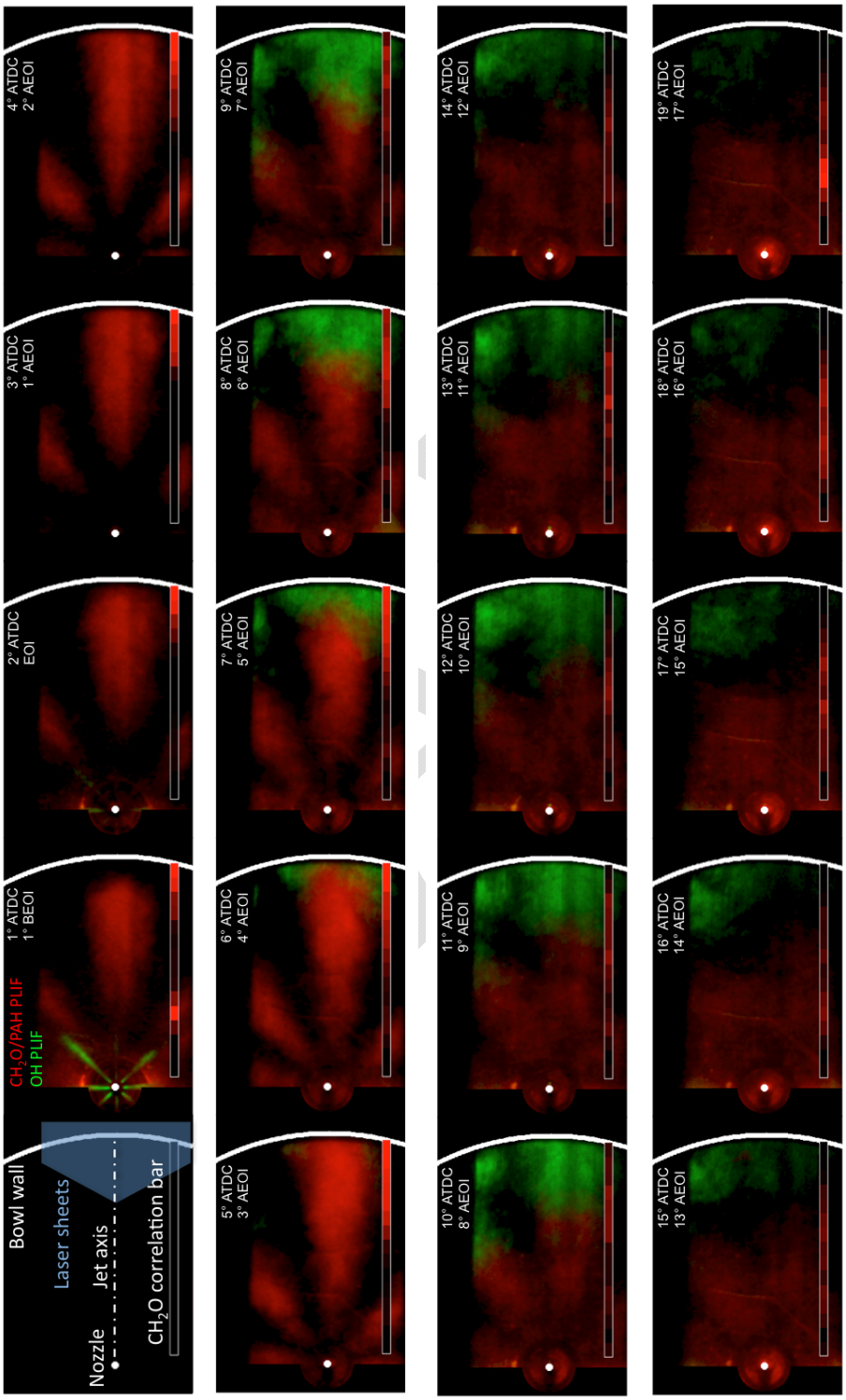

Figure A1. Combined results for OH-PLIF (green) and formaldehyde/PAH PLIF (red) with single main injection only. The configuration is given in the first frame and the timings indicated are relative to TDC and the main EOI. The formaldehyde correlation bar indicates the similitude of the formaldehyde/PAH PLIF signal to a formaldehyde reference spectrum. The darkest colors in the correlation bar indicate a low correlation with a formaldehyde reference spectrum whereas the brightest color indicate that the LIF signal has a high probability of being formaldehyde-LIF signal.

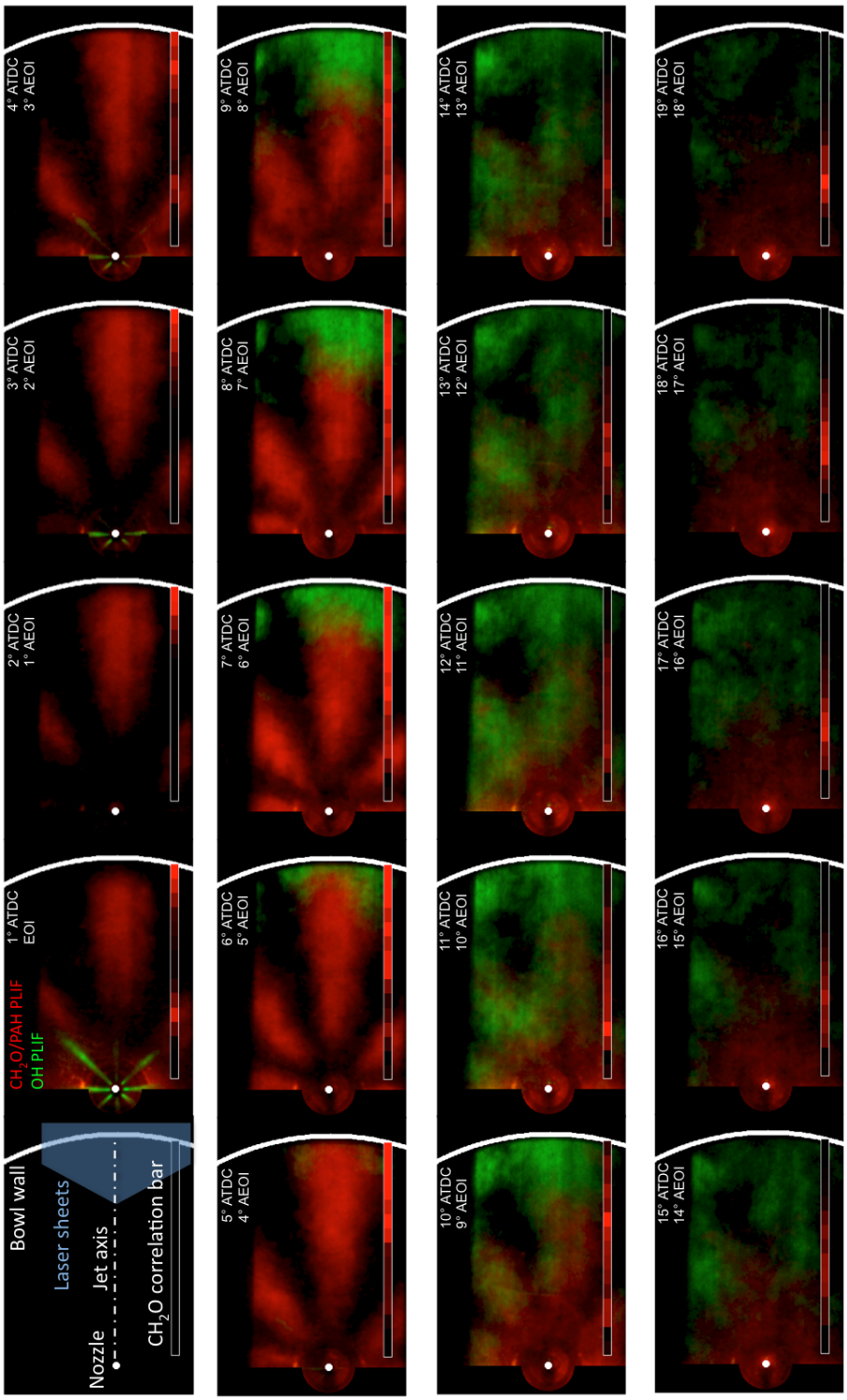

Figure A2. Combined results for OH-PLIF (green) and F/PAH PLIF (red) with main and small post- injection. See Fig. A1 for description of figure annotations.

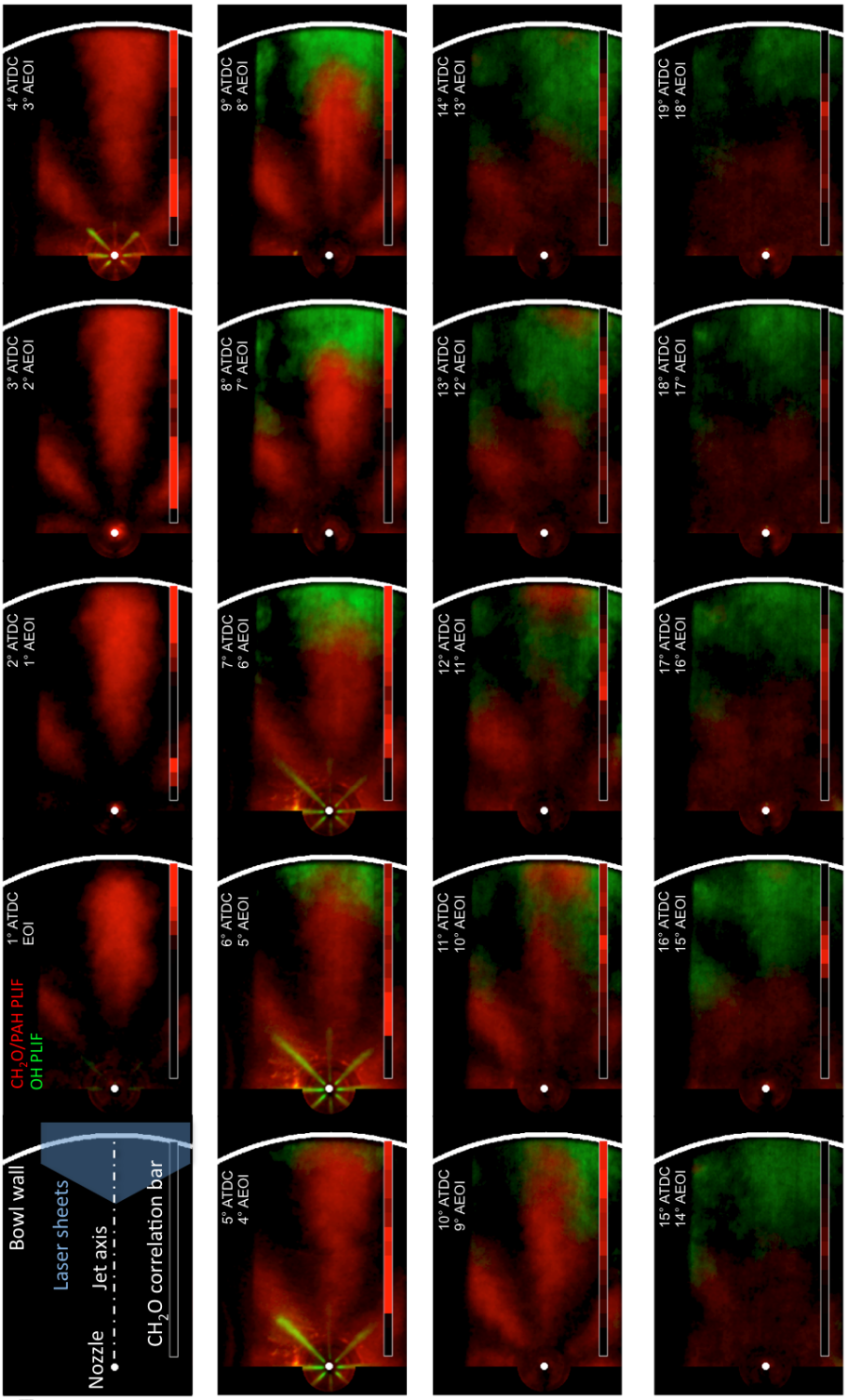

Figure A3. Combined results for OH-PLIF (green) and F/PAH PLIF (red) with main and large post- injection. See Fig. A1 for description of figure annotations.